Research Square

Preprints are preliminary reports that have not undergone peer review.
They should not be considered conclusive, used to inform clinical practice,
or referenced by the media as validated information.

Linoleic Acid Ameliorates Adenine-Induced CKD in Rats by Inhibiting Ferroptosis through the p38 MAPK and PPARα Pathways

Zelin Zhu
Zhejiang University of Technology
Yangyi Jiang
Zhejiang University of Technology
Haining Yu
yuhaining@zjut.edu.cn

Zhejiang University of Technology

Research Article

Keywords: Linoleic acid, Chronic kidney disease, Network pharmacology, Ferroptosis, MAPK

Posted Date: August 10th, 2026

DOI: https://doi.org/10.21203/rs.3.rs-10494747/v1

License: This work is licensed under a Creative Commons Attribution 4.0 International License.
Read Full License

Additional Declarations: No competing interests reported.

Abstract

Objective

This study investigated the protective effects of linoleic acid (LA) on adenine-induced chronic kidney disease (CKD) in rats and its underlying mechanisms.

Methods

A CKD rat model was established by oral gavage of 2.5% adenine, with LA and inulin as intervention and positive control, respectively. Renal function was evaluated by measuring serum blood urea nitrogen (BUN) and creatinine (Scr), and histopathology by hematoxylin and eosin (H&E) and Masson's trichrome staining. Triglycerides (TG), total cholesterol (T-CHO), low-density lipoprotein cholesterol (LDL-C), high-density lipoprotein cholesterol (HDL-C), TNF-α and IL-6 were determined using commercial assay kits. Levels of glutathione (GSH), malondialdehyde (MDA), superoxide dismutase (SOD), and iron were also measured. Protein expression of ACSL4, GPX4, and PTGS2 was examined by Western blotting. Network pharmacology and molecular docking predicted potential targets and signaling pathways, followed by Western blot validation of PPARα expression and p38 MAPK phosphorylation.

Results

LA significantly decreased levels of Scr and BUN, and attenuated renal histopathological injury, reversed dyslipidemia, and reduced TNF-α and IL-6 levels in CKD rats. LA also suppressed ferroptosis, as evidenced by decreased iron and MDA, increased GSH and SOD, decreased levels of ACSL4 and PTGS2, and upregulated expression of GPX4. Molecular docking revealed direct binding of LA to core targets including MAPK14 and PPARα. Western blot analysis confirmed that LA upregulated PPARα and inhibited p38 MAPK phosphorylation, thereby suppressing ferroptosis.

Conclusion

LA exerts protective effects in CKD rats by modulating ferroptosis through suppression of the p38 MAPK/ACSL4/PTGS2 pro-ferroptotic axis and activation of the PPARα/GPX4 anti-ferroptotic axis.

Introduction

Chronic kidney disease (CKD) is a highly prevalent and progressive renal disorder worldwide, characterized by complex and multi-factorial pathological mechanisms involving inflammation and lipid metabolism dysregulation[1–3]. Among these, dysregulated lipid metabolism has been increasingly recognized not merely as a consequence of CKD, but as an active contributor to its progression[4]. Accumulating clinical evidence demonstrates that CKD patients exhibit profound alterations in fatty acid

profiles, including elevated saturated fatty acids and reduced polyunsaturated fatty acid (PUFA) levels[5]. In parallel, chronic inflammation is a hallmark of CKD, with elevated levels of pro-inflammatory cytokines contributing to renal injury and fibrosis[6].

LA is an essential omega 6 PUFA that plays a critical role in maintaining metabolic homeostasis by regulating lipid metabolism[7, 8] and modulating inflammatory responses[9]. Notably, plasma and erythrocyte linoleic acid (LA) levels are consistently reduced in CKD patients compared to healthy individuals[10, 11], and insufficient dietary LA intake has been linked to adverse clinical outcomes[12]. In adenine-induced chronic tubulointerstitial nephropathy models, serum LA levels are markedly decreased, accompanied by significant alterations in fatty acid oxidation and LA metabolism[13]. These clinical and experimental observations suggest that LA deficiency may represent a metabolically and pathologically significant feature of CKD progression. Given that dyslipidemia and chronic inflammation are key pathological features of CKD, these properties of LA suggest that it may exert beneficial effects in CKD. However, whether LA supplementation can ameliorate lipid metabolism disorders and inflammatory responses in CKD, and whether such effects translate into renoprotection, remains largely unknown.

Importantly, the role of LA in CKD may extend beyond its metabolic and anti-inflammatory functions to involve the regulation of ferroptosis. Accumulating evidence has identified ferroptosis—a form of regulated cell death driven by iron-dependent lipid peroxidation[14]—as a key mechanism contributing to CKD progression[15, 16]. CKD models and patients exhibit hallmark features of ferroptosis, including iron accumulation[17], and dysregulated expression of ferroptosis-related proteins such as glutathione peroxidase 4 (GPX4)[18] and acyl-CoA synthetase long-chain family member 4 (ACSL4)[19]. LA occupies a unique and paradoxical position within this ferroptosis regulatory network. On one hand, as a PUFA, LA can be esterified into membrane phospholipids by ACSL4 and serve as a substrate for lipid peroxidation, thereby potentially promoting ferroptosis[20, 21]. On the other hand, LA and its metabolites have been reported to exert protective effects through maintaining membrane integrity, enhancing antioxidant capacity, and reducing oxidative stress[22]. Therefore, whether LA supplementation exerts renoprotective effects in CKD, and whether such effects involve the regulation of ferroptosis, remains largely unknown.

Therefore, in this study, we employed an adenine-induced rat model of CKD to investigate the effects of LA supplementation on renal function, lipid metabolism, inflammation, and ferroptosis, and to explore the underlying molecular mechanisms by which LA exerts its renoprotective effects.

Materials and Methods

Adenine-induced CKD model and LA treatment

Following 1 week of acclimatization, 50 Sprague–Dawley rats were weighed on day 7 and randomly assigned into two groups: control Check (CK) group (n = 10) and CKD model group (n = 40). From day 8, rats in the model group received a 2.5% adenine (Shanghai MacLean Biochemical Technology Co, Ltd)

suspension via gastric lavage once daily at a dose of 250 mg/kg(Based on previously reported adenine doses with minor modifications[23–25]). Rats in the CK group received saline once daily via gastric lavage. Both groups underwent continuous gastric lavage for 3 weeks.

Thirty-nine successfully modelled rats were randomly allocated into four groups: 1) CKD model (n = 10); 2) high-dose LA intervention (HLA, 0.6975 g/kg LA ,n = 10); 3) low-dose LA intervention (LLA, 0.4406 g/kg LA, n = 10); 4) positive control inulin (IN) (5.0000 g/kg IN, n = 9). Studies have shown that IN intake enhances antioxidant activity in the kidney tissue of rats with CKD, alleviates kidney damage, and slows disease progression[26]; therefore, IN was selected as the positive control in this study. Except for the CK group rats, rats in the remaining groups received a 2.5% adenine suspension once every 2 days at fixed intervals for modelling. Based on a basal dietary LA level of approximately 0.08 g/kg provided by standard chow, additional oral gavage resulted in total daily LA intakes of approximately 0.52 g/kg in the LLA group and 0.78 g/kg in the HLA group. By body surface area-based equivalent conversion, these doses correspond to daily intakes of approximately 5.0 g and 7.6 g LA, respectively, for a 60-kg adult. This dose range precisely covered the spectrum from the lower limit of the Acceptable Macronutrient Distribution Range for linoleic acid (approximately 5.0 g/d) to the Adequate Intake level (approximately 8.0 g/d) specified in the Chinese Dietary Reference Intakes, successfully simulating the dietary LA intake of the population from relatively low to adequate levels. All dosing regimens involved oral administration via gavage and lasted for 14 days, with daily weighing of rats prior to administration to adjust dosages according to real-time weight changes. Throughout the entire experiment, the same feed was used for feeding.

At the trial endpoint, serum was collected and organs (including the kidneys and liver) were removed for subsequent parameter measurements. The flowchart of CKD model establishment and treatment protocol is shown in Fig. 1.

H&E staining

Paraffin embedded kidney tissues were sectioned into 5 μm. Sections were dewaxed in xylene, rehydrated with gradient ethanol, and stained using a H&E staining kit (Shanghai Biyun Tian Biotechnology Co, Ltd, Shanghai, China). The staining patterns of the sections were examined under an optical microscope (Nikon Corporation, Tokyo, Japan), with corresponding images captured and analyzed to evaluate renal pathological damage scores.

Masson's trichrome staining

The kidney tissue sections were stained with acid fuchsin(Shanghai yuanye Bio-Technology Co, Ltd, Shanghai, China) and aniline blue solutions(Shanghai yuanye Bio-Technology Co, Ltd, Shanghai, China), which highlighted fibrotic areas in blue. A semiquantitative analysis of the blue-positive areas corresponding to fibrosis was performed using ImageJ software (ImageJ 1.8, NIH, USA).

Determination of renal function parameters

Serum creatinine (Scr) and blood urea nitrogen (BUN) levels were determined using the Creatinine Assay Kit and the Blood Urea Nitrogen Assay Kit, respectively (both obtained from Nanjing Jiancheng Bioengineering Institute, Nanjing, China). A microplate reader (BioTek, USA) was employed to measure Scr and BUN levels at 546 nm wavelength.

Determination of lipid metabolism indicators

The Triglyceride Assay Kit, Total Cholesterol Assay Kit, Low-Density Lipoprotein Cholesterol Assay Kit, and High-Density Lipoprotein Cholesterol Assay Kit (all obtained from Nanjing Jiancheng Bioengineering Institute, Nanjing, China) were used to determine triglyceride (TG), total cholesterol (T-CHO), low-density lipoprotein cholesterol (LDL-C), and high-density lipoprotein cholesterol (HDL-C) levels, respectively. A microplate reader was employed to measure TG, T-CHO, LDL-C, and HDL-C levels at 500, 500, 600, and 600 nm wavelength, respectively.

Serum inflammatory factor concentration testing

The Rat Interleukin-6(IL-6) Detection Kit and Rat Tumor necrosis factor-α (TNF-α) Detection Kit (both purchased from Shanghai Enzyme-Linked Bio-Technology Co, Ltd, Shanghai, China) were employed to determine IL-6 and TNF-α concentrations, respectively, in rat serum. IL-6 and TNF-α levels were measured at 450 nm wavelength.

Determination of ferroptosis-related indicators

The levels of Malondialdehyde (MDA), glutathione (GSH), total superoxide dismutase (SOD), and iron content were determined using the GSH Assay Kit, MDA Detection Kit, SOD Detection Kit, and Iron Content Assay Kit, respectively (all obtained from Nanjing Jiancheng Bioengineering Institute, Nanjing, China). A microplate reader was employed to measure GSH levels, MDA levels, SOD activity, and iron content at 420, 532, 550, and 520 nm, respectively.

Network pharmacology

The SMILES format of LA was obtained from the PubChem database (https://pubchem.ncbi.nlm.nih.gov/) and submitted to the SwissTargetPrediction platform (http://www.swisstargetprediction.ch/) for target prediction, with the species set to Homo sapiens and a probability threshold > 0.1. CKD-related targets were retrieved from the OMIM database (http://omim.org/), Therapeutic Target Database (https://db.idrblab.net/ttd/), and GeneCards database (https://www.genecards.org/). Ferroptosis-related targets were identified using the FerrDb database (http://www.zhounan.org/ferrdb/current/). Common targets among LA, CKD, and ferroptosis were

determined by intersection and imported into the STRING database (http://string-db.org/) to construct a protein–protein interaction (PPI) network. These common targets were further analyzed using Metascape for Gene Ontology (GO) and Kyoto Encyclopedia of Genes and Genomes (KEGG) pathway enrichment analysis.

Molecular docking between LA and the identified key targets was performed using AutoDock Vina and PyMOL. The 3D structure of LA was obtained from the PubChem Compound Database (https://pubchem.ncbi.nlm.nih.gov/), and the 3D structures of key target proteins were downloaded from the Protein Data Bank (PDB) database (http://www.rcsb.org/). Target proteins were prepared by removing water molecules and existing ligands and adding polar hydrogen atoms. LA was energy-minimized using ChemDraw 3D. All protein and molecular files were converted to PDBQT format using AutoDock Tools. Ligand–protein docking was performed using AutoDock Vina with a grid box encompassing the entire protein domain. Docking results were visualized using PyMOL.

Western blot analysis

Proteins were extracted from kidney tissue and quantified using the Bicinchoninic acid (BCA) Protein Assay Kit (Shanghai Biyun Tian Biotechnology Co, Ltd, Shanghai, China). Following SDS-PAGE separation using High Resolution Rapid Electrophoresis Buffer (Servicebio, Wuhan, China), proteins were transferred onto polyvinylidene fluoride (PVDF) membranes. Membranes were blocked with 5% non-fat milk for 2 h and incubated overnight at 4°C with primary antibodies: ACSL4 (1:5000), GPX4 (1:2000), Prostaglandin-endoperoxide synthase 2 (PTGS2) (1:2000), p38 Mitogen-activated Protein Kinase (MAPK) (1:2000), Phospho-p38 MAPK (Thr180/Tyr182) (1:2000), and Peroxisome proliferator-activated receptor alpha (PPARα) (1:2000) (all from Proteintech, Wuhan, China). After incubation with secondary antibodies, membranes were developed using enhanced chemiluminescence (ECL) reagent (Shanghai Biyun Tian Biotechnology Co, Ltd, Shanghai, China). Protein bands were visualized under light-protected conditions and quantified using ImageJ. Target protein levels were normalized to Glyceraldehyde-3-phosphate dehydrogenase (GAPDH) (1:2000) (Proteintech, Wuhan, China).

Statistical analysis

Data were analyzed using GraphPad Prism 8.0.1 software. Paired comparisons were performed using the t-test, while multiple comparisons were conducted via one-way analysis of variance. Results are presented as the mean ± standard error of the mean. Two-tailed p-values < 0.05 indicate statistically significant differences, while p-values < 0.01 denote highly significant differences.

Results

Establishment of a rat model of CKD

Following model establishment, rats in the CK group and CKD model group exhibited differences in coat condition, excretion volume, and mental state. Rats in the CKD model group showed markedly

deteriorated health, as indicated by yellowed, dry, and matted coats, lethargic behaviour, reduced activity levels, and increased bedding moisture. As sensitive indicators of renal injury, Scr and BUN accurately reflected impaired renal function in the CKD model group throughout this experiment. After modelling, the levels of BUN (Fig. 2a) and Scr (Fig. 2b) in the CKD model group were significantly lower than those in the CK group, suggesting that renal function in the model group had already become abnormal and that excretory capacity was impaired. H&E staining stained with haematoxylin and eosin (Fig. 2c) revealed normal renal tissue architecture in the CK group. The fundamental structural morphology of glomeruli, tubules, and renal interstitial remained distinct and unaltered, with no evident inflammatory cell infiltration in the renal interstitium. This indicates preserved renal function in this group, free from pathological damage. The renal tissue of the CKD model group exhibited marked structural abnormalities, specifically characterised by reduced interstitial vasculature, extensive inflammatory cell infiltration, and abnormal fibrous tissue proliferation. Glomeruli displayed numerous small vacuoles, a marked reduction in number accompanied by atrophy, and pronounced cystic dilatation. These alterations indicate chronic injury and inflammatory response in the kidneys of the CKD model group. Therefore, the above results confirm the successful establishment of an adenine-induced rat model of CKD.

LA ameliorates renal injury and dysfunction in CKD rats

Compared to the model group, renal morphology improved across all intervention groups, with kidneys exhibiting a more reddish hue, there were also significant differences in kidney index (Fig. 3a), reduced swelling, and decreased volume (Fig. 3b). Staining with H&E (Fig. 3d) revealed that the CKD model group exhibited mild glomerular lesions, compensatory tubular dilatation with incisions, substantial adenine brown crystal deposits within tubules, enlarged interstitial oedema vacuoles in glomeruli, and inflammatory cell infiltration. Across intervention groups, glomerular vacuoles exhibited varying degrees of reduction, luminal narrowing was observed, and inflammatory cell infiltration in renal interstitium was diminished. Moreover, xanthine brown crystal deposits were reduced compared to the CKD model group. These findings indicate that LA and IN interventions can effectively mitigate kidney damage and improve tubular and glomerular lesions. The results of Masson’s trichrome staining (Fig. 3e) revealed markedly increased blue areas indicative of fibrosis in the sections of rats from the CKD model group, signifying excessive extracellular matrix deposition and severe interstitial fibrotic damage. Compared to the CKD model group, all intervention groups exhibited reduced blue areas, reflecting varying degrees of diminished interstitial fibrosis. Further semi-quantitative analysis of the sections revealed reduced fibrotic areas in the LLA group compared to the CKD model group (Fig. 3c), indicating that LA intervention effectively mitigated renal fibrotic damage.

To investigate renal function across rat groups, we assessed the levels of BUN and Scr. As shown in Fig. 3f, by day 7 of intervention, blood BUN levels were significantly elevated in the CKD model group compared to the CK group. Following the administration of LA and IN, BUN levels were significantly lower in all intervention groups than in the CKD group. By day 14 of intervention, BUN levels were significantly reduced in all intervention groups compared to the CKD model group. Of note, there were no

significant difference between the levels of BUN in the intervention groups and those in the CK group. As depicted in Fig. 3g, Scr levels were significantly elevated in the CKD model group compared to the CK group by day 7 of intervention. In addition, Scr levels were significantly lower in the HLA intervention group than in the CKD group, there was no significant decrease in the other intervention groups. By day 14 of intervention, Scr levels in all intervention groups were significantly lower than those in the CKD model group. Scr levels in the intervention groups showed no significant difference compared to those in the CK group. In summary, these experimental results indicate that LA intervention effectively improved renal function in CKD model rats, demonstrating a positive therapeutic effect for CKD.

LA ameliorates dyslipidemia and suppresses inflammation in CKD Rats

To evaluate the effects of LA on lipid metabolism in rats with CKD, we measured lipid metabolism-related parameters including TG, T-CHO, LDL-C, and HDL-C. Compared to the CK group, the serum levels of TG (Fig. 4a), T-CHO (Fig. 4b), and LDL-C (Fig. 4d) were significantly elevated in the CKD model group, whereas those of HDL-C were reduced (Fig. 4c). These alterations indicate disrupted lipid metabolism in the CKD model group. Following intervention, the serum levels of TG, T-CHO, and LDL-C were significantly reduced in the HLA, LLA, and IN intervention groups compared to the CKD model group. However, no significant changes in serum HDL-C levels were observed across all intervention groups, and these levels remained significantly different from those detected in the CK group.

Serum IL-6 (Fig. 4e) and TNF-α (Fig. 4f) levels were higher in the CKD model group compared to the CK group, indicating a significant inflammatory response in CKD model rats. Following 14 days of intervention, serum IL-6 and TNF-α levels in the LA group showed a marked and statistically significant reduction compared to those measured in the CKD model group. In contrast, the IN intervention group showed a slight downward trend compared to the CKD model group, but the difference was not statistically significant.

LA suppresses ferroptosis in CKD rats

To investigate ferroptosis in rats across different groups, we assessed ferroptosis-related markers in the serum and kidneys, including GSH, MDA, SOD, and iron content. Compared to the CKD model group, the LLA group exhibited significantly elevated serum and renal GSH levels (Fig. 5a). In HLA intervention group, serum and renal SOD content markedly elevated (Fig. 5c). MDA levels in both renal tissue and serum were significantly reduced across all intervention groups compared to the CKD model group (Fig. 5b). Following intervention, serum iron levels were significantly elevated in both the HLA and LLA intervention groups compared to the CKD model group (Fig. 5d). In contrast, the renal iron content was significantly reduced in all intervention groups compared to the CKD model group (Fig. 5d). This suggests that rats in the CKD group exhibit iron metabolism disorders, with iron ions shifting from the serum to the kidneys and accumulating there. This iron imbalance may be associated with excessive iron uptake resulting from upregulated transferrin receptor 1(TFR1) expression in the kidneys[27, 28].

The reduction in renal iron content following LA treatment suggests that LA may mitigate ferroptosis partly by alleviating iron overload in the kidneys.

To investigate the potential mechanism, we examined the expression of ACSL4, GPX4, and PTGS2, three key regulators of ferroptosis, in renal tissues across all groups by western blotting. The results (Fig. 5e-Fig. 5g) showed that LA intervention downregulated the ferroptosis promoters ACSL4 and PTGS2 while upregulating GPX4, suggesting that LA may exert a protective effect against CKD by suppressing ferroptosis.

Network pharmacology analysis and Western blot validation of core targets

By screening databases for LA, CKD and ferroptosis-related targets, 27 functional targets were identified and plotted in a Venn diagram (Fig. 6a). A PPI network diagram was constructed (Fig. 6b and Fig. 6c), where larger nodes with darker colours indicate greater involvement in biological functions and stronger centrality. GO enrichment analysis was performed on the intersecting targets (Fig. 6d), with the top 10 enriched terms visualised as shown. The analysis indicated that LA-mediated ferroptosis in CKD primarily involves pathways such as regulation of inflammatory response and lipid oxidation. The KEGG analysis revealed enrichment across 80 signalling pathways (Fig. 6e), with top-ranked pathways including the serotonergic synapse pathway, PPAR signalling pathway, IL-17 signalling pathway, C-type lectin receptor signalling pathway, and TNF signalling pathway. These highly ranked pathways may represent the primary mechanisms through which LA treats CKD by regulating ferroptosis. Subsequently, we performed molecular docking between key target proteins and LA (Fig. 6f-Fig. 6l). The top two targets —MAPK14 and PPARα—may represent the primary action targets through which LA modulates ferroptosis to treat CKD.

Following the network pharmacology findings, molecular docking analysis revealed that MAPK14 and PPARα exhibited strong binding affinity with LA. To further validate the regulatory roles of these targets in CKD, we examined their protein expression in renal tissues by western blotting. The results (Fig. 7a - Fig. 7b) indicate that LA intervention upregulated PPARα protein expression while suppressing the excessive phosphorylation of p38 MAPK. These findings suggest that LA may exert a protective effect against CKD by modulating these key proteins, thereby attenuating ferroptosis. The proposed mechanism by which LA ameliorates CKD through ferroptosis suppression is illustrated in Fig. 8.

Discussion

This study demonstrates that LA significantly alleviates ferroptosis-associated pathological changes in adenine-induced CKD rats, accompanied by coordinated modulation of multiple key regulatory proteins. These results suggest that LA confers renoprotection through multi-target and multi-pathway regulation of ferroptosis.

In the present study, adenine administration induced a CKD phenotype characterized by severe dyslipidemia—elevated serum TG, T-CHO, and LDL-C—as well as increased BUN and Scr, and exacerbated renal interstitial fibrosis. LA treatment markedly reversed these biochemical and histopathological changes, demonstrating its capacity to restore lipid homeostasis, preserve renal function, and attenuate fibrotic remodeling. Consistent with previous reports that LA supplementation improves renal function in nephrectomized models[29], our findings extend these observations by demonstrating that LA also confers renoprotection in an adenine-induced CKD model.

Ferroptosis, which is intimately linked with the lipid metabolic disturbances characteristic of CKD[30], has been implicated in renal tubular injury[31]. In our study, CKD rats exhibited glutathione depletion, elevated malondialdehyde, and reduced superoxide dismutase activity, indicating a severe oxidant–antioxidant imbalance. Marked iron accumulation was also observed in renal tissue, creating a permissive microenvironment for ferroptosis. Importantly, LA intervention significantly ameliorated these alterations, indicating a close association between LA treatment and ferroptosis suppression. These data provide, to our knowledge, the first in vivo evidence linking LA intervention to ferroptosis suppression in a CKD model.

Although PUFAs are traditionally regarded as lipid peroxidation substrates and potential ferroptosis promoters in vitro[32], our findings reveal a context-dependent protective effect of LA in CKD. We propose that under chronic metabolic stress, LA may act primarily as a signaling-modulating lipid rather than a passive peroxidation substrate. Specifically, LA may reshape ferroptosis sensitivity through nuclear receptor signaling and stress kinase pathways, thereby shifting the balance toward cytoprotection.

To explore the underlying mechanisms, we combined network pharmacology with in vivo validation and identified MAPK14 (p38α), PPARα, and PTGS2 as potential targets associated with LA activity. Based on these predictions, we further examined ferroptosis-related signaling and propose that LA operates through a bidirectional regulatory network: suppressing pro-ferroptotic signals while activating antioxidant defense pathways.

On the pro-ferroptotic side, ACSL4 promotes incorporation of PUFAs into membrane phospholipids to generate polyunsaturated fatty acid-containing phosphatidylethanolamine species, enhancing ferroptosis susceptibility[33]. PTGS2 is widely used as a downstream marker of ferroptosis[34]. In CKD rats, both ACSL4 and PTGS2 were markedly upregulated, and LA treatment significantly suppressed their expression, consistent with reduced ferroptotic sensitivity.

At the upstream signaling level, p38 MAPK phosphorylation was substantially increased in CKD rats, while total p38 expression remained unchanged, indicating pathway activation. Given that MAPK14 was predicted as an LA target and that p38 activation has been linked to ferroptosis promotion[35], our data suggest that LA may attenuate ferroptosis partly by inhibiting p38 MAPK activation. Whether LA acts directly on p38 or indirectly via upstream nuclear receptors remains to be clarified.

On the anti-ferroptotic side, GPX4 functions as a central enzyme that detoxifies lipid peroxides and constitutes a core defense mechanism[36]. GPX4 expression was significantly reduced in CKD rats but was restored by LA treatment, indicating enhanced antioxidant capacity.

PPARα, a key nuclear receptor that regulates lipid metabolism and inflammation[37], also emerged as a potential mediator of LA action. PPARα activation has been reported to reduce the accumulation of oxidizable lipid species and suppress ferroptosis susceptibility[30]. In line with this, LA significantly upregulated PPARα expression, which paralleled GPX4 restoration, suggesting a coordinated PPARα–GPX4 axis that contributes to ferroptosis resistance.

Taken together, these findings support a dual regulatory model in which LA simultaneously suppresses the p38 MAPK/ACSL4/PTGS2 pro-ferroptotic axis and activates the PPARα/GPX4 antioxidant axis, thereby restoring redox balance and mitigating renal injury in CKD. This model suggests that LA functions not merely as a metabolic substrate, but as a bioactive lipid signaling regulator under conditions of chronic oxidative stress.

This study provides preclinical evidence supporting the potential application of LA in CKD management. Given its essential nature, wide availability, and favorable safety profile[38], LA may represent a promising nutritional intervention strategy for CKD.

This study also has several limitations that should be noted. First, the proposed mechanistic model is based primarily on correlative evidence; causal relationships require further validation using pharmacologic inhibitors and genetic manipulation of p38 MAPK and PPARα pathways. Second, this study used only the adenine-induced model, which limits generalizability; validation in additional models, such as 5/6 nephrectomy or unilateral ureteral obstruction, is warranted. Third, several targets predicted by network pharmacology were not experimentally verified at the protein level. Finally, the optimal LA dosing regimen, therapeutic window, and translational applicability require systematic investigation.

Conclusion

This study provides in vivo evidence linking LA intervention to the attenuation of ferroptotic phenotypes in the kidneys of adenine-induced CKD rats. The underlying mechanism may involve suppression of the p38 MAPK/ACSL4/PTGS2 pro-ferroptotic axis and activation of the PPARα/GPX4 anti-ferroptotic axis. These findings offer new mechanistic insights and preclinical evidence supporting the potential use of LA as a nutritional intervention strategy for CKD.

Abbreviations

ACSL4 Acyl
CoA synthetase long-chain family member 4

Declarations

Ethical approval

All experimental procedures were conducted in accordance with the National Institutes of Health (NIH) guidelines for the care and use of laboratory animals (NIH publication No. 85 – 23, revised 1996), and were approved by the Zhejiang University of Technology Laboratory Animal Ethics Committee (Approval No. MGS20230329035), ensuring scientific rigour and ethical compliance.

Consent for publication

Not Applicable.

Informed consent

Not Applicable.

Consent to participate

Not Applicable.

Competing interests

The authors declare no competing interests.

Funding

No funding was received for conducting this study.

Author Contribution

Zelin Zhu: Conceptualization, Data curation, Methodology, Software, Writing–original draft; Yangyi Jiang: Data curation, Formal analysis, Investigation, Writing–original draft, Writing- Reviewing and Editing; Haining Yu: Supervision, Writing- Reviewing and Editing.

Data availability

No datasets were generated or analysed during the current study.

Code availability

not applicable.

References

1. Kanbay M, Copur S, Bakir CN, Covic A, Ortiz A, Tuttle KR. Glomerular hyperfiltration as a therapeutic target for ckd. Nephrol Dialysis Transplantation. 2024;39:1228–38. https://doi.org/10.1093/ndt/gfae027.
2. Miguel V, Shaw IW, Kramann R. Metabolism at the crossroads of inflammation and fibrosis in chronic kidney disease. Nat Rev Nephrol. 2025;21:39–56. https://doi.org/10.1038/s41581-024-00889-z.
3. Theofilis P, Vordoni A, Koukoulaki M, Vlachopanos G, Kalaitzidis RG. Dyslipidemia in chronic kidney disease: Contemporary concepts and future therapeutic perspectives. Am J Nephrol. 2021;52:693–701. https://doi.org/10.1159/000518456.
4. Mitrofanova A, Merscher S, Fornoni A. Kidney lipid dysmetabolism and lipid droplet accumulation in chronic kidney disease. Nat Rev Nephrol. 2023;19:629–45. https://doi.org/10.1038/s41581-023-00741-w.
5. Gu X, Dong YD, Wang XM, Ren ZG, Li GH, Hao YX, et al. Identification of serum biomarkers for chronic kidney disease using serum metabolomics. Ren Fail. 2024;46. https://doi.org/10.1080/0886022X.2024.2409346.
6. Zhou R, Chen J, Xia B, Chen M, Zhu Y, Li G. Research progress on the treatment of renal injury with esculetin: Multi-target pharmacological mechanism and clinical translation prospect. Int J Mol Sci 2026;27. https://doi.org/10.3390/ijms27125465
7. Spartano NL, Lamon-Fava S, Matthan NR, Obin MS, Greenberg AS, Lichtenstein AH. Linoleic acid suppresses cholesterol efflux and atp-binding cassette transporters in murine bone marrow-derived macrophages. Lipids. 2014;49:415–22. https://doi.org/10.1007/s11745-014-3890-y.
8. Bowen KJ, Kris-Etherton PM, West SG, Fleming JA, Connelly PW, Lamarche B, et al. Diets enriched with conventional or high-oleic acid canola oils lower atherogenic lipids and lipoproteins compared to a diet with a western fatty acid profile in adults with central adiposity. J Nutr. 2019;149:471–8. https://doi.org/10.1093/jn/nxy307.
9. Lee KJ, Ko YJ, Kang SK, Kim WS, Cho CS, Choi YJ. Additive anti-inflammation by a combination of conjugated linoleic acid and α-lipoic acid through molecular interaction between both compounds. Food Sci Biotechnol. 2020;29:419–29. https://doi.org/10.1007/s10068-019-00677-7.
10. Khor BH, Narayanan SS, Chinna K, Gafor AHA, Daud ZAM, Khosla P et al. Blood fatty acid status and clinical outcomes in dialysis patients: A systematic review. Nutrients 2018;10. https://doi.org/10.3390/nu10101353
11. George C, Hill J, Nqebelele NU, Motshwari DD, Peer N, Kengne AP et al. Differences in red blood cell fatty acid profiles by type 2 diabetes status in early-stage chronic kidney disease. Sci Rep 2026;16. https://doi.org/10.1038/s41598-026-36504-3
12. Chen H, Yang QR, Yu FJ, Shen YX, Xia H, Yang MF, et al. Protective effect of unsaturated fatty acids on cognitive impairment in ckd patients: Results from the national health and nutrition examination

survey (2011–2014). Technol Health Care. 2024;32:3579–93. https://doi.org/10.3233/THC-240671.

13. Chen DQ, Chen H, Chen L, Vaziri ND, Wang M, Li XR, et al. The link between phenotype and fatty acid metabolism in advanced chronic kidney disease. Nephrol Dialysis Transplantation. 2017;32:1154–66. https://doi.org/10.1093/ndt/gfw415.
14. Dixon SJ, Lemberg KM, Lamprecht MR, Skouta R, Zaitsev EM, Gleason CE, et al. Ferroptosis: An iron-dependent form of nonapoptotic cell death. Cell. 2012;149:1060–72. https://doi.org/10.1016/j.cell.2012.03.042.
15. Yasam SK, Vignesh N, Rajagopal S. Advances in ferroptosis research and applications. Int Rev cell Mol biology. 2026. https://doi.org/10.1016/bs.ircmb.2025.12.004. 405:149 – 86.
16. Liu KX, Yu M, He YY, Wang T, Li GS, Wang L et al. Inhibitory effects of herbal monomers on ferroptosis in renal fibrosis: A review and mechanistic study. Front Pharmacol 2025;16. https://doi.org/10.3389/fphar.2025.1610573
17. Liu KX, Yu M, He YY, Li Y, Huang XR, Li GS, et al. Smad3 mediates renal fibrosis via gpx4-dependent ferroptosis. Int J Biol Sci. 2025;21:5922–35. https://doi.org/10.7150/ijbs.114075.
18. Ursini F, Maiorino M. Lipid peroxidation and ferroptosis: The role of gsh and gpx4. Free Radic Biol Med. 2020;152. https://doi.org/10.1016/j.freeradbiomed.2020.02.027. :175 – 85.
19. Gao XL, Chen T, Lin SL, Guo CY, Li WJ, Ning WJ, et al. Quercetin alleviates folic acid-induced renal fibrosis by inhibiting tubular epithelial cell ferroptosis via egfr/acsl4 pathway. Am J Chin Med. 2025;53:1913–31. https://doi.org/10.1142/S0192415X25500715.
20. Ding KY, Liu CB, Li L, Yang M, Jiang N, Luo SL, et al. Acyl-coa synthase acsl4: An essential target in ferroptosis and fatty acid metabolism. Chin Med J. 2023;136:2521–37. https://doi.org/10.1097/CM9.0000000000002533.
21. Huang H, Chen YL, Yin N, Li GJ, Ye SS, Guo L, et al. Unsaturated fatty acid liposomes selectively regulate glutathione peroxidase 4 to exacerbate lipid peroxidation as an adaptable liposome platform for anti-tumor therapy. Mol Pharm. 2023;20:290–302. https://doi.org/10.1021/acs.molpharmaceut.2c00642.
22. Wang C, Wang RJ, Hu LJ, Xi MC, Wang MJ, Ma YJ, et al. Metabolites and metabolic pathways associated with allelochemical effects of linoleic acid on < i> karenia < i> mikimotoi. J Hazard Mater. 2023;447. https://doi.org/10.1016/j.jhazmat.2023.130815.
23. Zhang CY, Zhu JY, Ye Y, Zhang M, Zhang LJ, Wang SJ, et al. Erhuang formula ameliorates renal damage in adenine-induced chronic renal failure rats via inhibiting inflammatory and fibrotic responses. Biomed Pharmacother. 2017;95:520–8. https://doi.org/10.1016/j.biopha.2017.08.115.
24. Zhang ZM, Yang L, Wan Y, Liu C, Jiang S, Shang EX, et al. Integrated gut microbiota and fecal metabolomics reveal the renoprotective effect of rehmanniae radix preparata and corni fructus on adenine-induced ckd rats. J Chromatogr B-Analytical Technol Biomedical Life Sci. 2021;1174. https://doi.org/10.1016/j.jchromb.2021.122728.
25. Wang J, Zhang QB, Jin WH, Niu XZ, Zhang H. Effects and mechanism of low molecular weight fucoidan in mitigating the peroxidative and renal damage induced by adenine. Carbohydr Polym.

2011;84:417–23. https://doi.org/10.1016/j.carbpol.2010.11.055.

26. Melekoglu E, Cetinkaya MA, Kepekci-Tekkeli SE, Kul O, Samur G. Effects of prebiotic oligofructose-enriched inulin on gut-derived uremic toxins and disease progression in rats with adenine-induced chronic kidney disease. PLoS ONE. 2021;16. https://doi.org/10.1371/journal.pone.0258145.
27. Annamalai C, Viswanathan P. Iron biology in acute kidney injury: Catalytic iron, hepcidin-ferroportin axis, and ngal-a narrative review. Int J Mol Sci. 2026;27. https://doi.org/10.3390/ijms27093802.
28. Shihab EM, Abbas SN, Shareef SM, Hasan RJ, Alsaraf KM, Fawzi HA. Azilsartan as a novel anti-ferriptotic agent via the upregulation of the nrf2/ho-1/slc7a11/gpx4 axis and downregulation of inflammatory pathways in folic acid-induced acute kidney injury in male mice. Toxicol Rep. 2026;16:102204. https://doi.org/10.1016/j.toxrep.2026.102204.
29. Heifets M, Morrissey JJ, Purkerson ML, Morrison AR, Klahr S. Effect of dietary lipids on renal function in rats with subtotal nephrectomy. Kidney Int. 1987;32:335–41. https://doi.org/10.1038/ki.1987.214.
30. Xin S, Schick JA. Pufas dictate the balance of power in ferroptosis. Cell Calcium. 2023;110. https://doi.org/10.1016/j.ceca.2023.102703.
31. Ma SJ, Han Q, Li J, Wang HY, Wang YM, Bai XY, et al. Mesenchymal stem cells attenuate diabetic nephropathy by suppressing the erk-ferroptosis-ros axis. Int J Mol Sci. 2026;27. https://doi.org/10.3390/ijms27115101.
32. Wang N, Wang J, Wu YF, Qu ML, Hong JW, Cui ZY et al. Cynarin counteracts lipotoxicity in pancreatic β-cells via inhibiting palmitate-induced apoptosis and linoleic acid-provoked ferroptosis. Plant Foods Hum Nutr 2025;80. https://doi.org/10.1007/s11130-025-01382-z
33. Shao NJ, Tan KB, Chen P, Luo Q. Acsl4 mediates ferroptosis to promote immunoglobulin a nephropathy progression: Scrna-seq analysis. Sci Rep. 2026;16. https://doi.org/10.1038/s41598-026-43023-8.
34. Jiang YL, Hui DC, Pan ZY, Yu YX, Liu L, Yu XF, et al. Curcumin promotes ferroptosis in hepatocellular carcinoma via upregulation of acsl4. J Cancer Res Clin Oncol. 2024;150. https://doi.org/10.1007/s00432-024-05878-0.
35. Huang F, Li WR, Li J, Ran YH, Fu SY, Shen L, et al. Depleted uranium exposure induced ferroptosis in renal cells via the ethe1/p38-mapk pathway. Arch Toxicol. 2026;100:465–74. https://doi.org/10.1007/s00204-025-04221-x.
36. Shi ZD, Zhang C, Xie T, Song J, Zeng XQ, Hu JY, et al. Molecular mechanisms and therapeutic strategies of gpx4 regulation in acute kidney injury. Pharmacol Rep. 2026;78:218–35. https://doi.org/10.1007/s43440-025-00777-8.
37. Yuan SL, Liu JX, Wu JY, He JH, Qiu LW. Exercise attenuates high-fat diet-induced liver injury in mice via pparα pathway and reduction of oxidative stress and inflammation. J Physiol Biochem 2026;82. https://doi.org/10.1007/s13105-026-01167-1
38. Patro-Golab B, Zalewski BM, Kammermeier M, Schwingshackl L, Koletzko B. Int Union Nutr Sci I. Fat intake and fat quality in pregnant and lactating women, infants, children, adolescents and related

health outcomes: A scoping review of systematic reviews of prospective studies. Annals Nutr Metabolism. 2023;79:413–22. https://doi.org/10.1159/000533757.

Figures

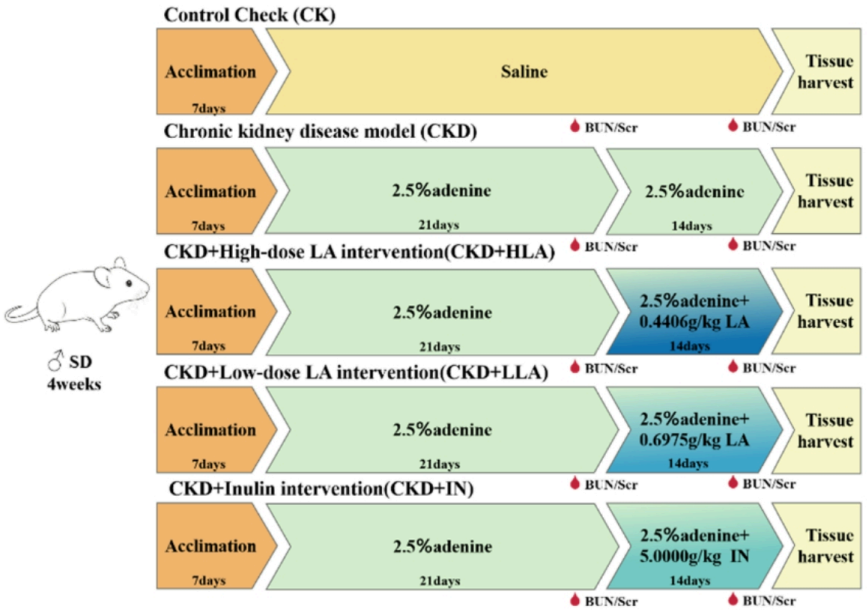


Figure 1

CKD model construction and intervention flow chart.CK: Control Check, n = 9; CKD: Chronic kidney disease,n = 10; CKD+HLA: High-dose LA intervention, n = 10; CKD+LLA: Low-dose LA intervention, n = 10; CKD+IN: Inulin intervention, n = 9

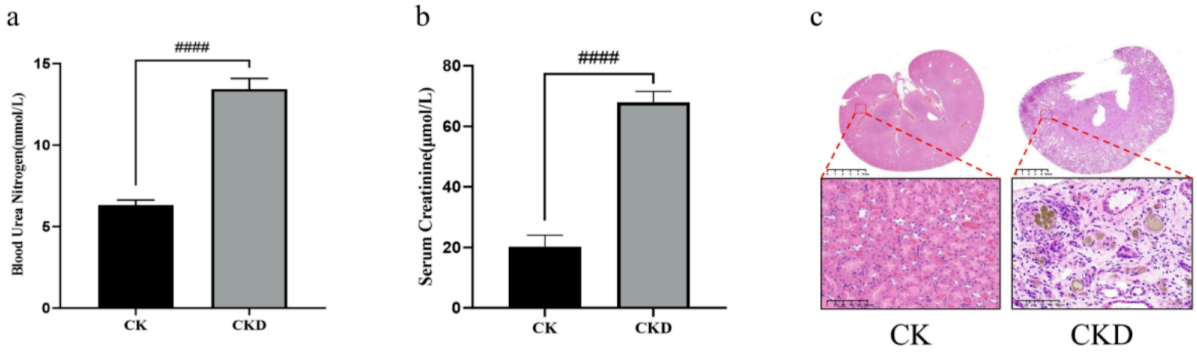


Figure 2

A rat model of CKD was successfully established by adenine administration, as evidenced by impaired renal function and characteristic histopathological injuries. (a, b): Serum levels of renal function markers: blood urea nitrogen (BUN, a) and serum creatinine (Scr, b). (c): Representative hematoxylin and eosin (H&E) stained Micrographs of kidney tissue, demonstrating the histopathological injuries induced by adenine. Compared with CK, $^{\#\#\#\#}P < 0.0001$. CK, n = 10; CKD, n=40

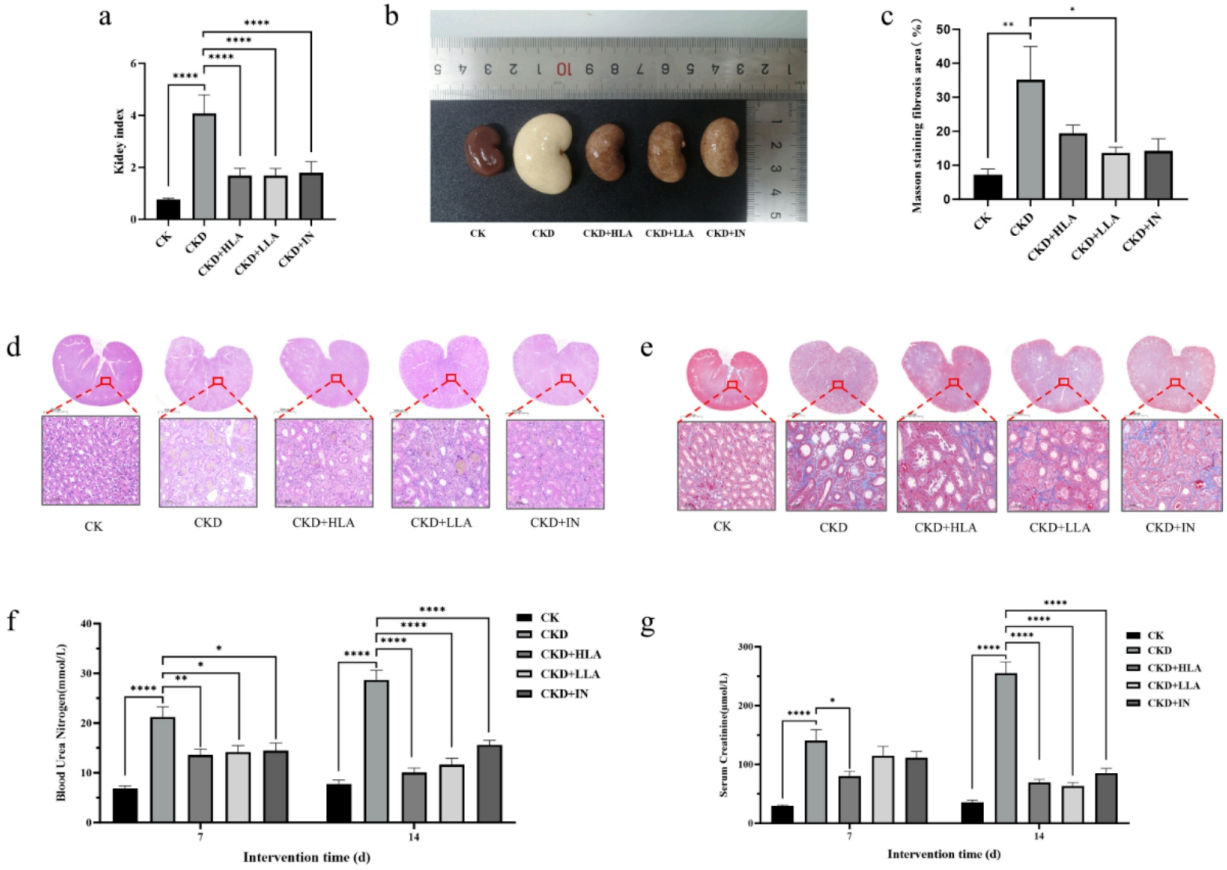


Figure 3

LA treatment alleviated renal dysfunction, histopathological changes, and fibrosis in CKD rats. (a): Kidney index, calculated as the ratio of kidney weight to final body weight. (b): Representative gross images of kidneys. (c): Semi-quantitative analysis of the fibrotic area based on (e). (d): Representative hematoxylin and eosin (H&E) stained sections of kidney tissue. (e): Representative Masson's trichrome stained sections of kidney tissue. (f, g): Levels of renal function markers in serum: blood urea nitrogen (BUN, f) and serum creatinine (Scr, g).Compared with CKD, *$P < 0.05$, **$P < 0.01$, ****$P < 0.0001$. Figure 2a: CK, n = 9; CKD, n = 10; CKD+HLA, n = 10; CKD+LLA, n = 10; CKD+IN, n = 9. Figure 2c: n = 4. Figure 2f-2g: n = 6

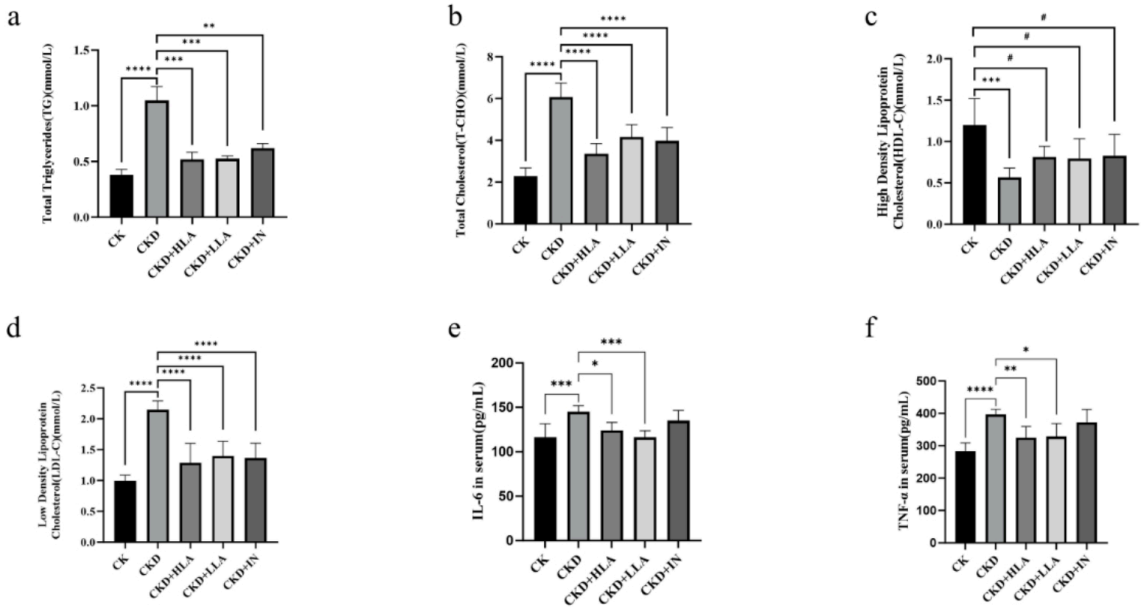


Figure 4

LA attenuates biochemical and molecular disturbances in CKD Rats by improving lipid metabolism and suppressing inflammation. (a-d): Serum levels of lipids: triglycerides (TG, a), total cholesterol (T-CHO, b), high-density lipoprotein cholesterol (HDL-C, c), and low-density lipoprotein cholesterol (LDL-C, d). (e, f) Serum levels of inflammatory cytokines: interleukin-6 (IL-6, e) and tumor necrosis factor-alpha (TNF-α, f).Compared with CKD, **P* < 0.05, ***P* < 0.01, ****P* < 0.001, *****P* < 0.0001. Compared with CK, $^{\#}P$ < 0.05.n = 6

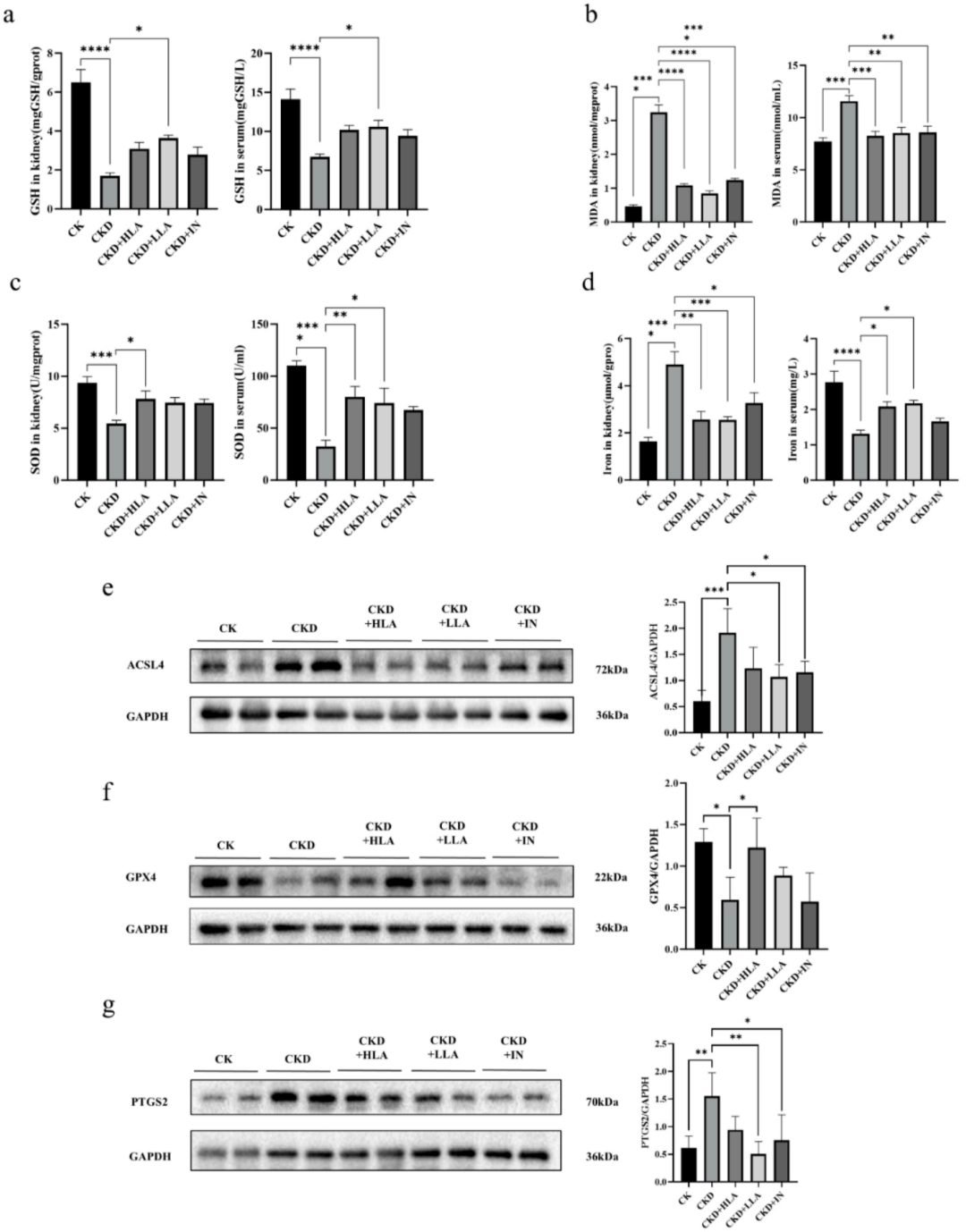


Figure 5

LA attenuates ferroptosis in CKD rats.(a-d): Detection of ferroptosis-related indicators in serum and renal tissues: glutathione (GSH, a), malondialdehyde (MDA, b) levels, superoxide dismutase (SOD, c) activity andIron content (d). (e-g): Western blot analysis of ACSL4, GPX4, and PTGS2 protein expression in renal tissues: ACSL4(e), GPX4(f), and PTGS2(g).Compared with CKD, *$P < 0.05$, **$P < 0.01$, ***$P < 0.001$, ****$P < 0.0001$. Figure 5a-5d:n = 6. Figure 5e-5g:n = 4

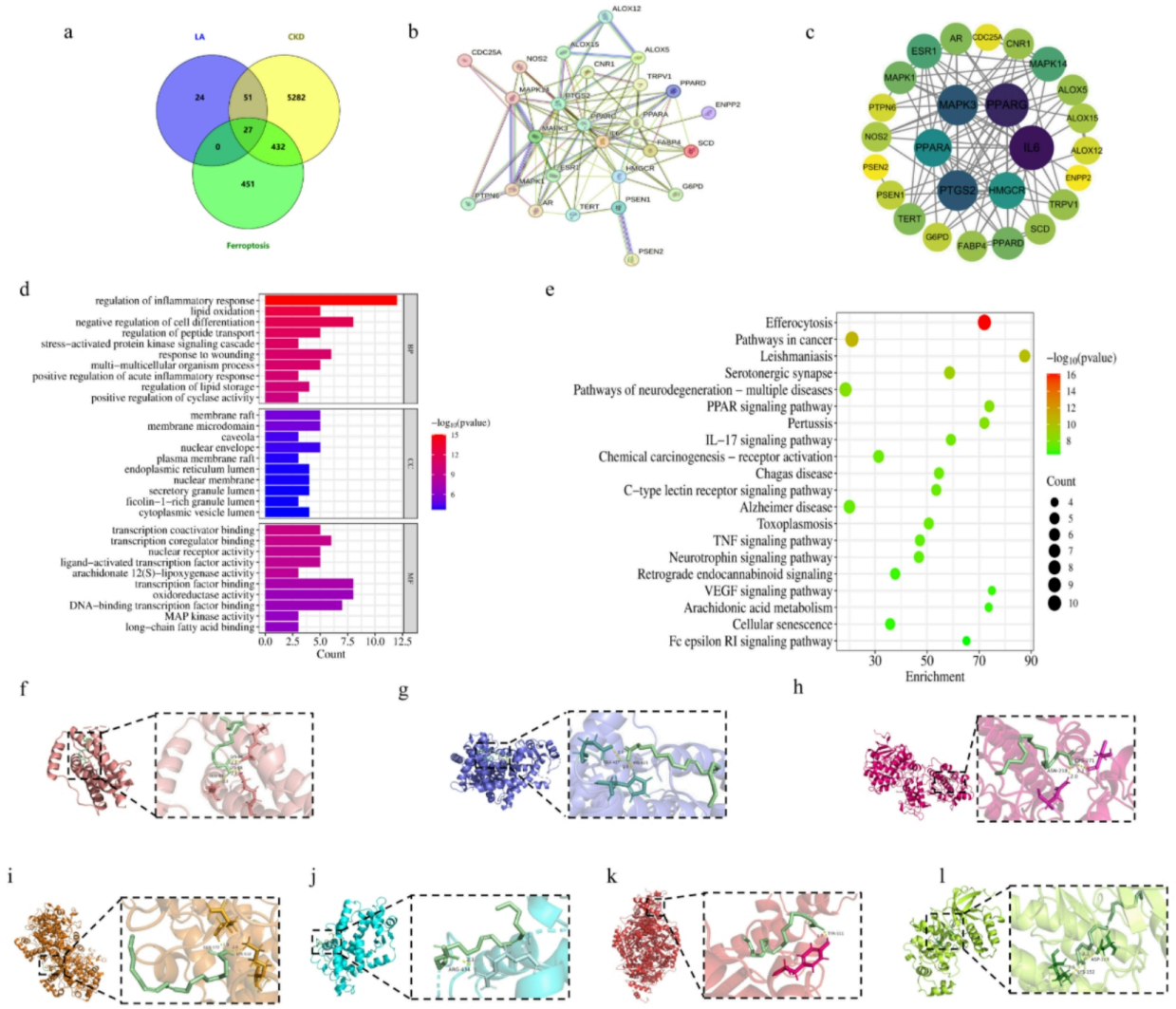


Figure 6

Integrated network pharmacology and molecular docking identify ferroptosis-related targets and associated pathways as potential mechanisms of LA action in CKD. (a): Venn diagram identifying the overlapping targets among LA, CKD and ferroptosis. (b, c): The protein-protein interaction network constructed from the overlapping ferroptosis-related targets (b) and its core subnetwork (c). (d, e): Functional enrichment analysis of the core targets, including Gene Ontology functional(d) and the KyotoEncyclopedia of Genes and Genomes pathway (e). (f-l): Molecular docking models illustrating the predicted binding poses and interactions between LA and the core protein targets: IL-6 (f), PPARG (g), MAPK3 (h), PTGS2 (i), PPARα (j), HMGCR (k), and MAPK14 (l)

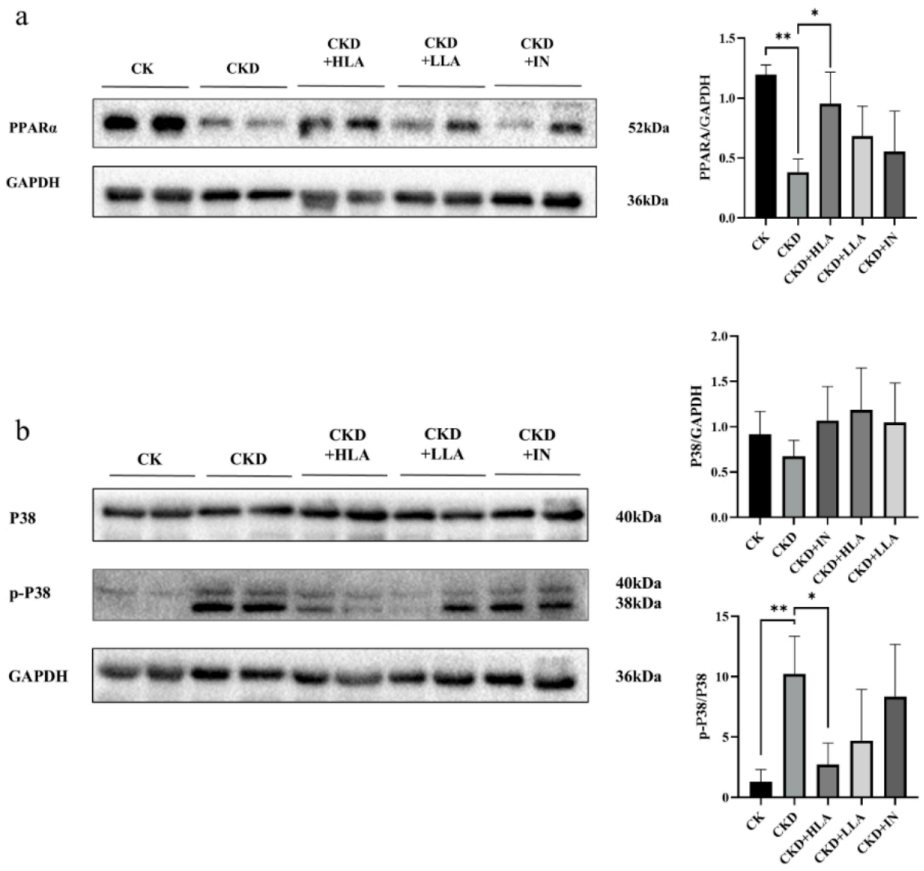


Figure 7

Western blot analysis detected the expression of the two target proteins with the highest binding affinities predicted by network pharmacology in renal tissues. (a,b): Representative Western blot images and quantitative analysis showing the protein expression levels of PPARα (a) and the phosphorylation ratio of P38 MAPK (p-P38/P38) (b) in the same model. Compared with CKD, *$P < 0.05$, **$P < 0.01$, ***$P < 0.001$. n = 4

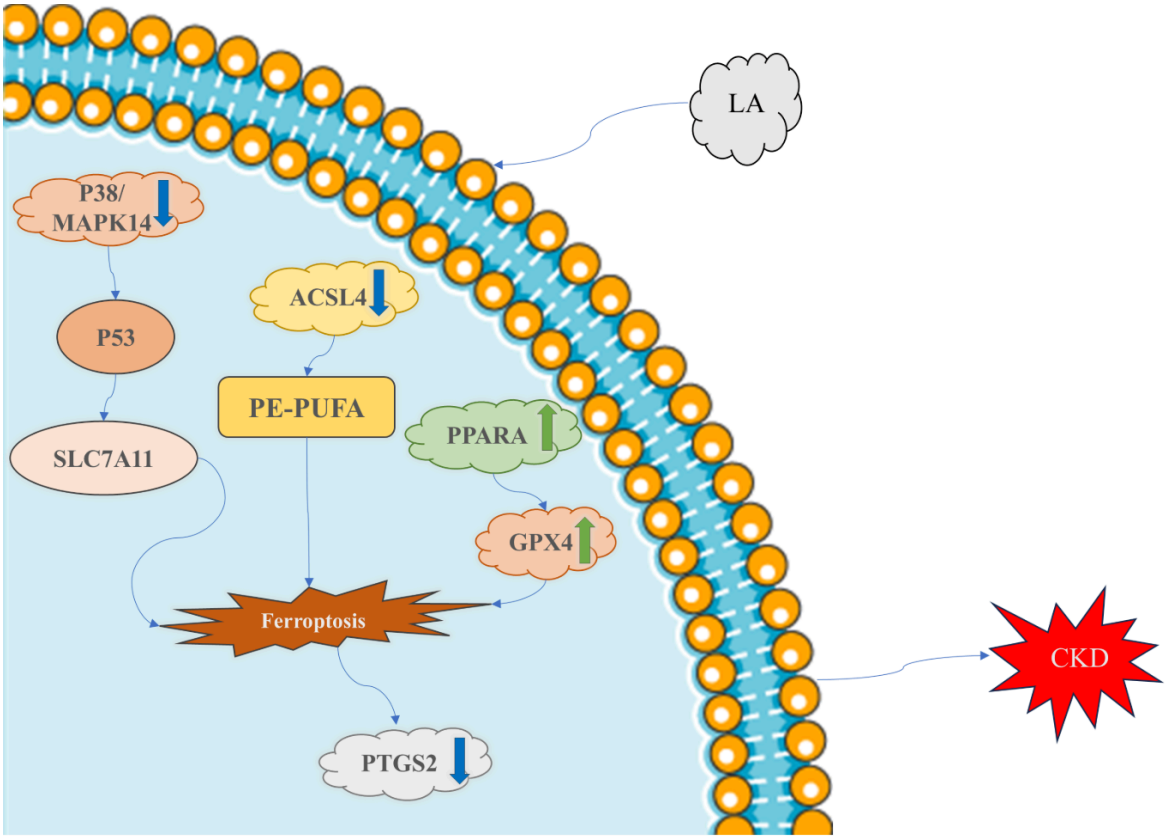


Figure 8

LA attenuates ferroptosis in the kidneys of CKD rats through coordinated regulation of multiple key targets. LA downregulates ACSL4, thereby limiting PUFA esterification and reducing the substrate availability for subsequent lipid peroxidation; upregulates GPX4 to enhance the clearance of phospholipid hydroperoxides; restores PPARα expression, which improves lipid metabolism and antioxidant defense; reduces PTGS2 protein levels, a well-established downstream marker of ferroptosis, in line with the suppression of ferroptosis; and inhibits P38 MAPK phosphorylation, thereby blocking the p53/SLC7A11-mediated pro-ferroptotic signaling cascade. Collectively, these coordinated actions alleviate oxidative stress, restore redox homeostasis, and ultimately protect against ferroptosis-associated renal injury in CKD

Supplementary Files

This is a list of supplementary files associated with this preprint. Click to download.

- supplementaryfile.docx